Novel β-Cyclodextrin Functionalized Core-Shell Fe_3O_4 Magnetic Nanoparticles for the Removal of Toxic Metals from Water

Babak Kaboudin,[a]* M. Torabi Momen[a], Foad Kazemi[a] and Priyanka Ray[a,b]

[a]Department of Chemistry, Institute for Advanced Studies in Basic Sciences, No. 444, Yousef Sobouti Blv, 45195-1159 Zanjan, Iran

[b]Department of Coatings and Polymeric Materials, North Dakota State University, Fargo, ND 58102, USA

Abstract

Herein we report the synthesis and characterization of β-CD functionalized core-shell Fe_3O_4 magnetic nanoparticles which were used as an adsorbent for removal of Lead (II) and Copper (II) ions from aqueous solution. Various characterization techniques including FTIR, TGA analysis, SEM, TEM, X-Ray diffraction patterns (XRD) and nitrogen adsorption- desorption measurements were employed to investigate the properties of the synthesized material. The influence of pH, contact time, metal ion concentration, adsorbent dosage of Lead (II) and Copper (II) ion removal were also studied. The isotherm models for both ions showed a fit to the Langmuir model. Thermodynamic parameters such as enthalpy, entropy and Gibbs free energy were also evaluated and the negative values of ΔH for both Lead (II) and Copper (II) ions indicated the exothermic nature their sorption.

Keywords:metal ion removal, purification,magnetic nanoparticles, cyclodextrin

1. Introduction

The accumulation of heavy metals in the environment has been a cause of major concern worldwide. This is primarily due to the extreme toxicity of metals at minimal concentrations that can be hazardous even in the sub nanomolar range and are responsible for causing life threatening diseases and severe damage to the environment.[1, 2] Moreover, metal contaminants are usually non-biodegradable and can neither be metabolized nor decomposed. Several methods for the removal of heavy metal ions have been investigated and include adsorption,[3, 4] ion exchange,[5, 6] solvent extraction,[7, 8] reverse osmosis,[9] photocatalysis,[10] precipitation,[11]and electrochemical[12] processes.

Nanoparticles have attracted huge attention over the past few decades owing to their unique size and shape dependent properties which vary largely from the bulk.[13-15] Soft and hard nanomaterials ranging from one to several hundred nanometres in size have been reported for their use in various domains including sensing, molecular recognition, drug delivery, imaging, catalysis, photovoltaics and even electronic devices.[16-39] In this regard, metal nanoparticles have been exploited for their optical, magnetic, conducting, and electronic properties.

Magnetic nanoparticles in particular have been employed as biosensors, imaging agents and for the removal of environmental pollutants. The most commonly employed methods for generating these nanoparticles include radiolytic, chemical, microwave, sonochemical and hydrothermal synthesis. However, magnetite (Fe_3O_4) is relatively unstable and quite sensitive to oxidation as it is easily converted to maghemite (γ-Fe_2O_3) in the presence of oxygen. Hence, it is essential to modify the surface of the materials to avoid aggregation and agglomeration, enhance dispersibility and increase their reactivity.

Surface modifications can be achieved via chemical modification using functional groups like carboxylicacid,[40] thiols, [41] porphyrin, [42] amino acids, [43] or by the addition of a layer of polymers, [44] alumina, [45] and silica.[46] Compared to organic coatings, silica has been found to be stable under acidic conditions and unlike polymers, it is chemically inert and does not exhibit any swelling or porosity change on its surface in response to a change in the environmental pH.[47] The surface of MNPs has also been functionalized with macromolecules such as calixarenes, crown ethers and cyclodextrins due to the macrocyclic properties of these compounds which have a stabilizing effect of the entire entity along with the stabilization of the magnetic core. The unique host-guest type interactions and the variation in ring sizes and chemical groups thus make them attractive candidates for surface functionalization[48-53].

Cyclodextrins, are a series of cyclic oligosaccharides composed of glucopyranose units joined by α-(1-4) linkage, forming a torus shaped structure. The ring structure of these compounds can be varied and thus used to entrap guests of selected size thus giving rise to various intra and intermolecular interactions to form stable host-guest type complexes. We have harnessed this attractive feature of this class of compounds and used a class of modified cyclodextrins for functionalization of magnetic nanoparticles for selective entrapment of Cu^{2+} and Pb^{2+} ions.

In this study, we aimed to fabricate an effective sorbent based on Fe_3O_4 magnetic nanoparticles and β-cyclodextrins. The synthesized MNPs were protected against agglomeration and oxidation, surface functionalization was achieved by adding (3-aminopropyl) triethoxysilane (APTES) followed by the grafting of cyclodextrin on to the amino functionalized MNPs. The functionalized MNPs were then used for the effective removal of heavy metal ions from aqueous solutions.

2. Experimental section

2.1 Materials

All materials used were of analytical grade and used without any purification. Ferric chloride hexahydrate ($FeCl_3 . 6H_2O$), ferrous chloride tetrahydrate ($FeCl_2 . 4H_2O$), ammonium hydroxide solution (25 W%), P- toluenesulfonyl chloride (TsCl), imidazole (Im), β-cylodextrin, tetraethyl ortho silicate (TEOS), (3-aminopropyl) triethoxysilane (APTES), acetic acid, sodium acetate trihydrate, sodium nitrate, nitric acid, copper(II) nitrate trihydrate and lead(II) nitrate were purchased from Sigma Aldrich. De-ionized (doubly distilled water) was used in all experiments.

2.2 Experimental procedure

2.2.1 Synthesis of Fe_3O_4 magnetic nanoparticles (MNPs) and silica coated magnetic nanoparticles (SMNPs): MNPs were synthesized by employing using the co-precipitation method in an alkaline solution using a 1:2 molar ratio of ferrous and ferric saltsas described in literature.[54] This was followed by the gradual addition of a solution of ammonium hydroxide, which resulted in a colour change from orange to black. The reaction mixture was allowed to stir for 30 minutes and the suspension was left to cool to room temperature. The MNPs thus produced were washed using de-ionized water and acetone, collected through magnetic decantation and were dried in a vacuum at 50 °C.

$$FeCl_2.4H_2O + 2FeCl_3.6H_2O + 8NH_4OH \longrightarrow Fe_3O_4(s) + 8NH_4Cl + 20\ H_2O$$

Coating of silica on the MNPs surface was achieved modifying a previously reported method.[55] Briefly, 150 mL ethanol was added to 1 g of Fe_3O_4 MNPs and sonicated for 40 minutes at room temperature. While stirring, 6 mL of concentrated ammonia solution and 2 mL TEOS were added and stirring continued for 24 hours. The silica coated MNPs were washed with ethanol and acetone and collected using an external magnet followed by vacuum drying at room temperature.

2.2.2 Synthesis of amino functionalized silica coated magnetic nanoparticles (AMNPs)

Amino functionalized silica coated magnetic nanoparticles were prepared using (3-aminopropyl) triethoxysilane (APTES) following the protocol reported by Kobayashi et al.[56] 1 g of SMNPs was added to anhydrous toluene and ultrasonically dispersed for 20 minutes. 0.5 mL APTES was added afterwards and stirring continued for 24 hours under nitrogen atmosphere. The precipitate was washed with ethanol and acetone several times and dried under vacuum for subsequent usage.

2.2.3 Synthesis of 6-O-toluenesulfonyl-β-cyclodextrin (6-O- β-CD)

6-O-toluenesulfonyl-β-cyclodextrin was prepared using a previously reported methods with some modifications.[57] 2.6 g imidazole was dissolved in 10 mL dry CH_2Cl_2 and then cooled to 0 °C in an ice bath. A solution of 3.2 g *p*- toluenesulfonyl chloride in 15 mL dry CH_2Cl_2 was added drop wise during 90 minutes to the solution. After attaining room temperature, stirring continued for 2 hours. The resultant suspension was extracted using CH_2Cl_2 (dichloromethane) and water (2 × 25 mL) and upon removal of the solvent in vacuo, white solid crystals of Ts-Im were isolated. Ts-Im Melting point: 75.5- 78.5 °C (lit.[53] 78-78.5 °C).

^{1}H NMR ($CDCl_3$, 400 MHZ): δ (ppm) 2.46 (s, 3 H), 7.10 (s, 1 H), 7.29 (s, 1H), 7.38 (d, 2H, *J*= 8.3), 7.83 (d, 2H, *J*= 8.3), 8.03 (s, 1H); **IR (cm $^{-1}$):** 3433, 3031, 2523, 1590, 1456, 1378, 1163, 1044, 669, 590.

3 g of hydrated β-CD was dissolved in 70 mL H_2O by heating at 60 °C and vigorous stirring. Ts-Im (2.3 g) was added to solution after cooling to room temperature under continuous stirring. After 2 hours a solution of 1.3 g sodium hydroxide in 2.7 mL H_2O was added for 20 minutes. After 10 minutes the un-reacted Ts-Im was separated through a sintered glass funnel. The reaction was quenched by adding 3.6 g ammonium chloride. The resulting mixture was left overnight and 6-O-toluenesulfonyl-β-cyclodextrinwhich precipitated at the bottom of liquid was collected through filtration using a sintered glass funnel and washed with ice water and acetone and vacuum dried.

^{1}H NMR (DMSO-d_6 400 MHZ): δ (ppm) 2.49 (s, 3 H), 3.20-3.65 (m, 40 H), 4.15-4.20 (m, 1 H), 4.30-4.38 (m, 2 H), 4.44-4.57 (m, 2 H), 4.51(br s, 3H), 4.76 (br s, 2H), 4.83 (br s, 4H), 5.62-5.83 (m, 1H), 7.42 (d, 2H, J= 8.1), 7.73 (d, 2H, J= 8.1); **IR (cm^{-1}):** 3394, 2926, 1642, 1414, 1159, 1033, 525.

2.2.4 Preparation of β-cyclodextrin grafted amino functionalized magnetic nanoparticles (β-CD MNPs)

The preparation of β-cyclodextrin grafted amino functionalized magnetic nanoparticles is analogous to the method described by Belyakova et *al.* with some modifications.[58] 15 mL anhydrous DMF was added to 1g amino functionalized MNPs and sonicated for 20 minutes. While stirring in an oil bath at 80 °C, 0.5 g 6-O- β-CD in 10 mL anhydrous DMF was added dropwise to the suspension. The reaction was stirred for 24 hours under argon atmosphere and the prepared β-CD MNPs were then washed with DMF, ethanol and acetone. They were then collected using an external magnet and dried under vacuum.

The process of fabricating β-cyclodextrin functionalized core-shell magnetic nanoparticles is shown schematically in Fig 1.

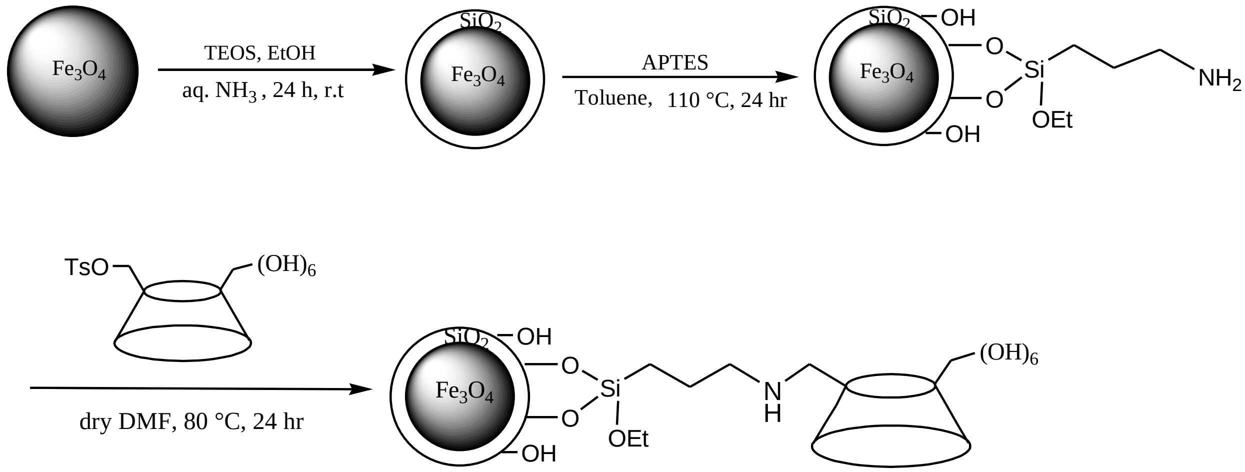

Figure 1 Schematic representation of the synthesis of β-cyclodextrin functionalized core-shell magnetic nanoparticles

3. Results and discussion

3.1 Synthesis and characterization of magnetic nanoparticles (MNPs)

The FTIR spectra of Fe_3O_4 MNPs, SMNPs, AMNPs and β-CD MNPs are shown in Fig. 2. Absorption at 574 cm^{-1} is the characteristic peak of Fe-O bonds. Formation of silica shell on the surface of MNPs is confirmed by the existence of stretching absorptionof Si-O-Si at 1088 cm^{-1}as reported in literature.[59]

Absorption of Si-OH stretching, Si-O- bending and Si-O-Si bending are also observed at 968, 801 and 462 cm^{-1} respectively. The same set of absorptions can be observed in the AMNPs spectra with slight shift, probably due to modification. Absorption at 2924 and 2880 cm^{-1} are assigned to the stretching vibrations of C-H bonds in aminopropyl groups and the absorption at 1627 cm^{-1} is attributed to N-H vibration.

Characteristic peaks of β-CD MNPs observed at 1200-900 cm^{-1} are related tothe antisymmetric glycosidic (C-O-C) vibrations and the coupled (C-C/C-O) stretching vibrations[60]which are shadowed by stretching absorption of Si-O-Si at 1088 cm^{-1}. Comparison between FTIR spectra of Fe_3O_4 MNPs, SMNPs, AMNPs and β-CD MNPs provides evidence of the successful surface modification of MNPs, which is further supported by thermogravimetric (TGA) analysis.

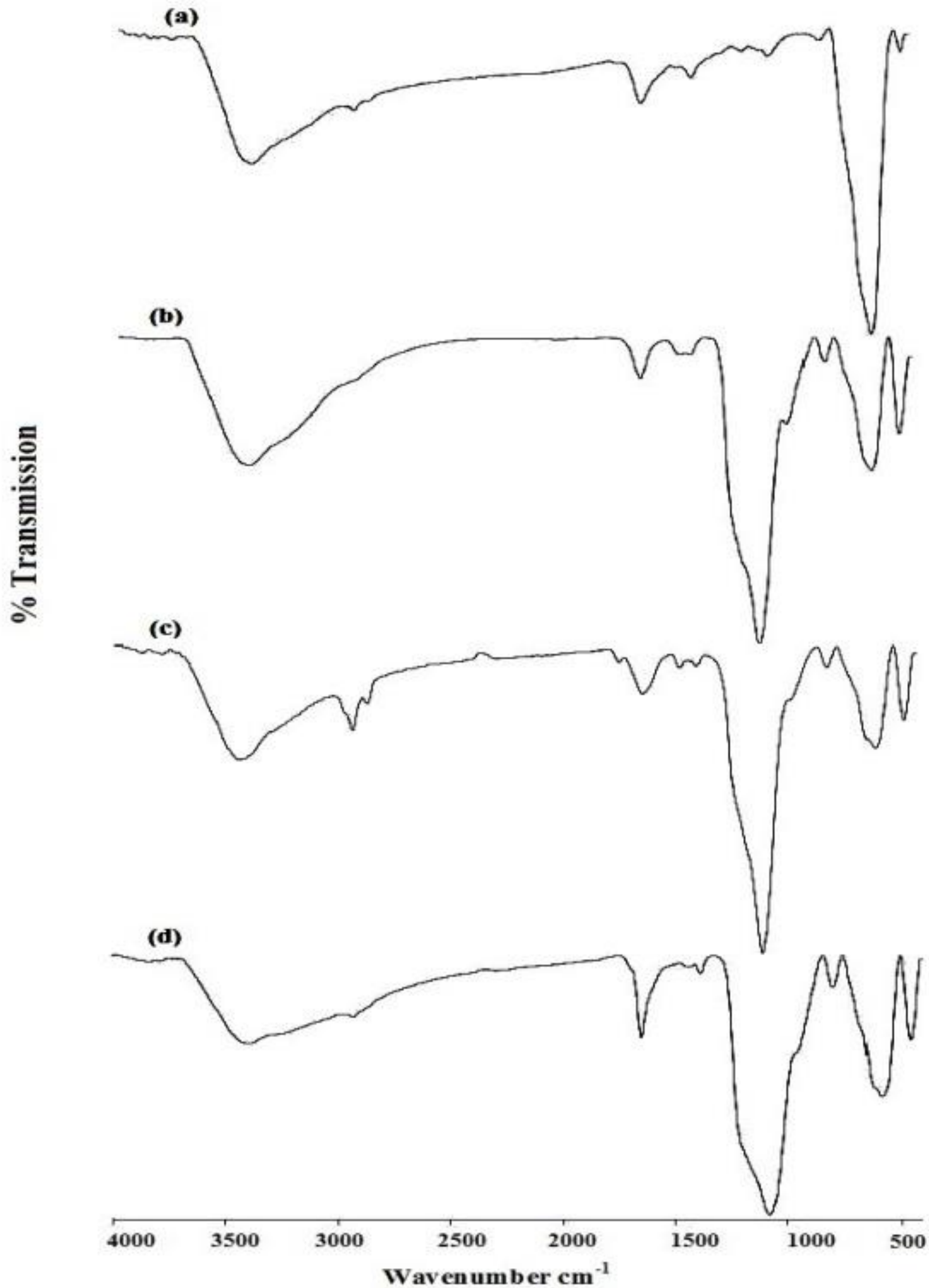

Figure 2. FTIR spectra of (a) Fe_3O_4 MNPs, (b) SMNPs, (c) AMNPs and (d) β-CD MNPs

TGA analysis was also used to determine the amount of organic content functionalized on the surface of MNPs. The first weight loss in TGA curves of bare MNPs and SMNPs is related to the loss of adsorbed solvents including water and ethanol, while the second weight loss is due to the dehydration of OH groups on the surface of bare MNPs and SMNPs. In the TGA curves of AMNPs and β-CD MNPs weight loss due to the evaporation of adsorbed solvents can also be observed. The 5.19% and 9.59% weight loss in TGA curves of AMNPs, β-CD MNPs indicates that the amount of grafted aminopropyl groups and β-CD on the surface of MNPs is equal to 0.894 and 0.039 mmol/g respectively (Fig. 3).

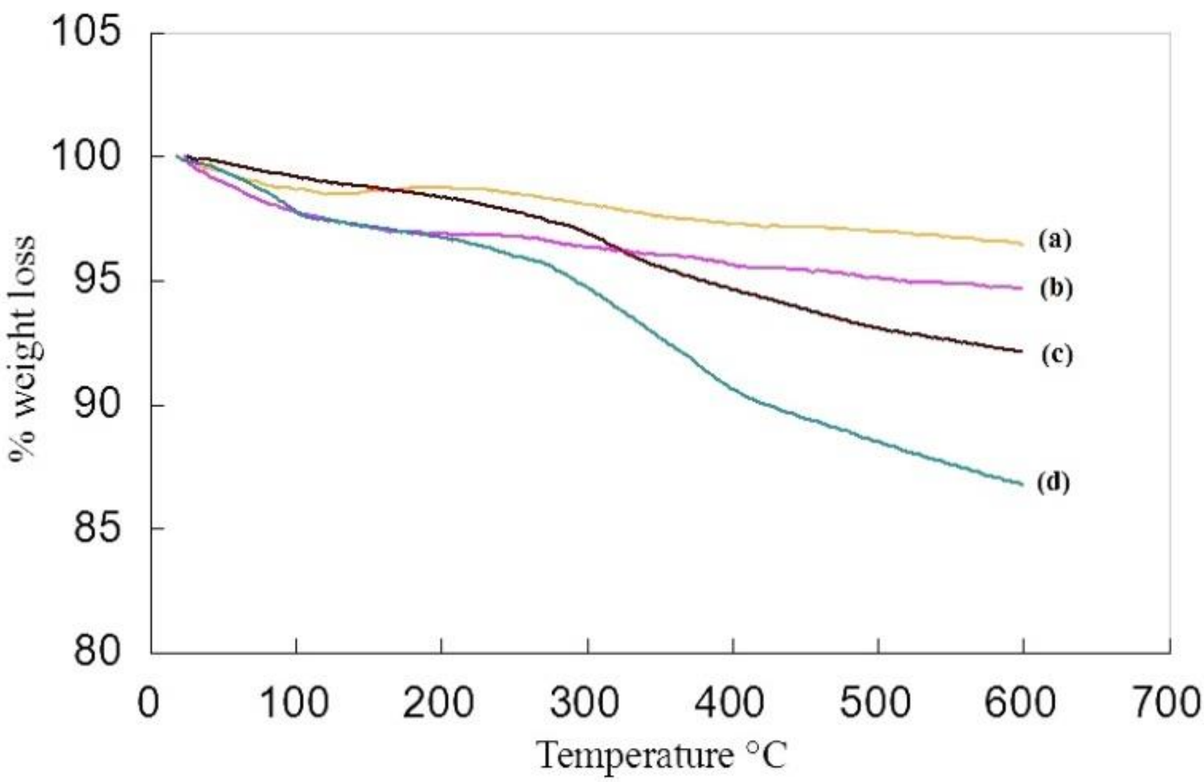

Figure 3. TGA curves of (a) Fe_3O_4 MNPs, (b) SMNPs, (c) AMNPs and (d) β-CD MNPs

In the XRD pattern of Fe_3O_4, characteristic peaks at 2θ= 31, 36, 43.5, 54, 57, 63 were observed and indicate the purity of the synthesized MNPs and their cubic spinel structure.[60] The same peaks are observed for SMNPs, AMNPs and β-CD MNPs as well, which confirm the fact that the surface modification process did not induce any phase change. The slightly broad and flattened peak at 2θ= 20 is due to the presence of the amorphous silica shell. Average crystal size of nanoparticles is calculated from the most intense peak by Debye-Scherrers formula ($D_{hkl} = 0.9\lambda/(\beta \cos \theta)$, λ is the X-Ray wavelength (0.154 nm), β expresses the half width of XRD diffraction lines and θ is the half diffraction angle of 2h.). Average crystal size of Fe_3O_4 MNPs and SMNPs were determined to be 15 and 21nm respectively.

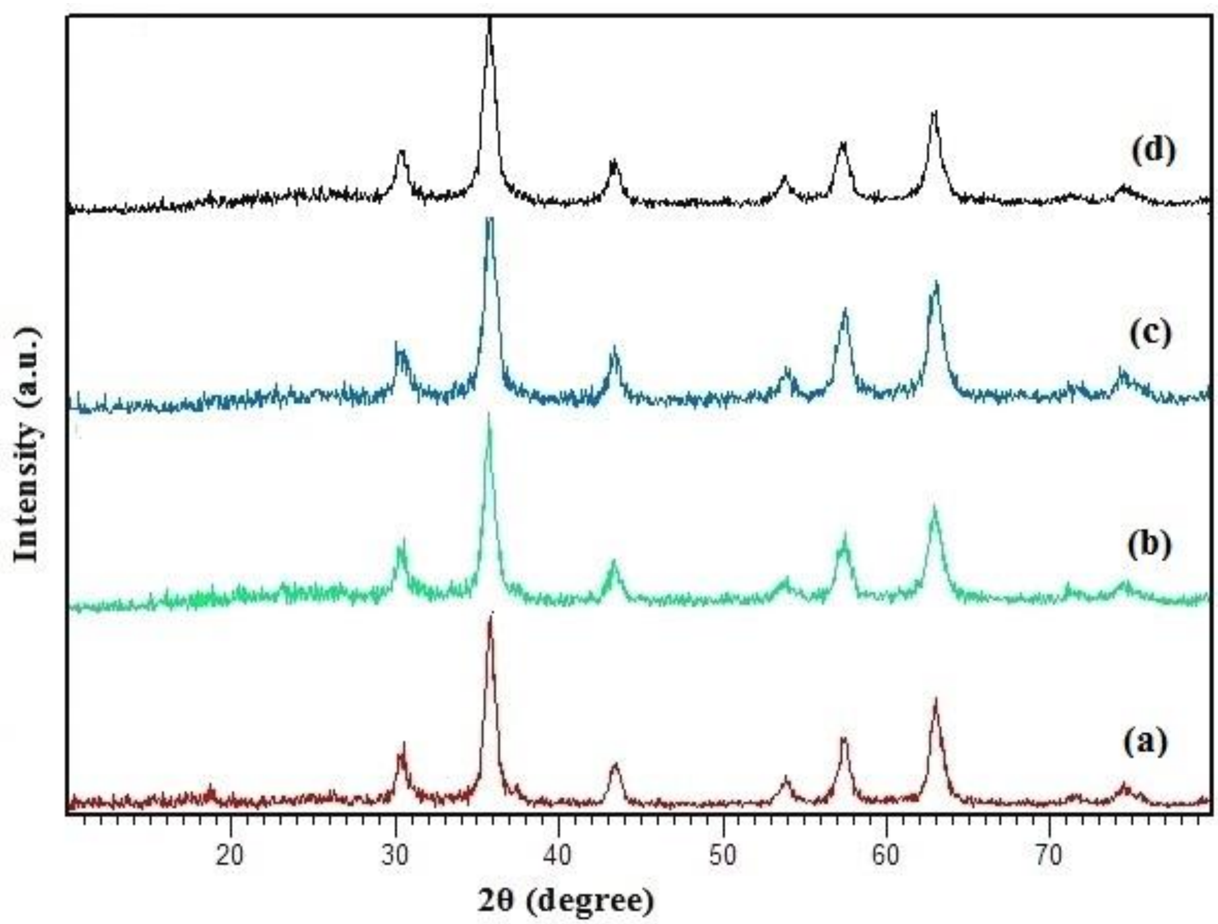

Figure 4. XRD patterns of (a) Fe_3O_4 MNPs, (b) SMNPs, (c) AMNPs and (d) β-CD MNPs

In the magnetization diagram of Fig. 5, saturations of 65, 41, 39.9 and 39 are related to Fe_3O_4 MNPs, SMNPs, AMNPs and β-CD MNPs respectively. No coercivity and remanence were observed in either sample, which proved the existence of superparamagnetic properties in all synthesized MNPs. Although silica coating of MNPs resulted in tangible decrease in saturation magnetization, owing to their superparamagnetic properties, both Fe_3O_4 MNPs and SMNPs could be easily recovered by an external magnet (Figure 6). Amino functionalization and β-CD grafting did not lead to a sizeable decrease in saturation.

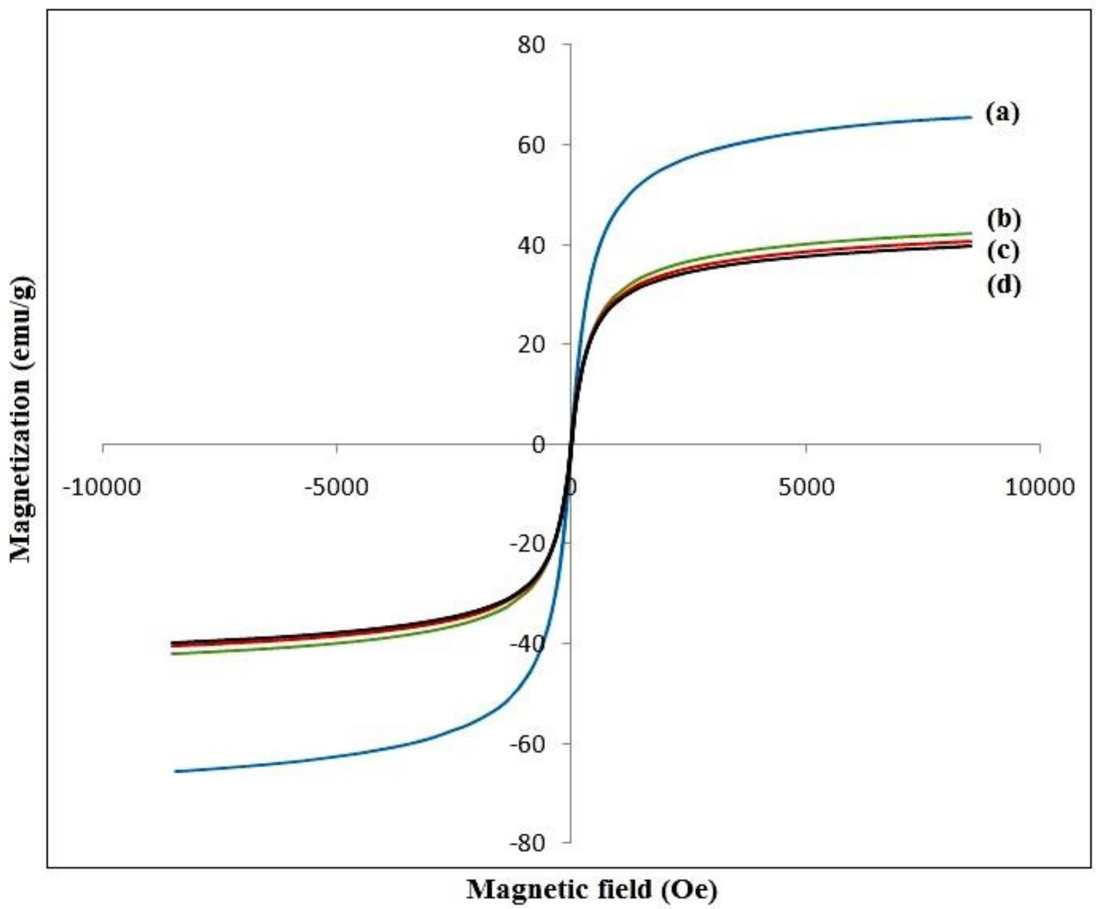

Figure 5. Magnetization curves of (a) Fe_3O_4 MNPs, (b) SMNPs, (c) AMNPs and (d) β-CD MNPs

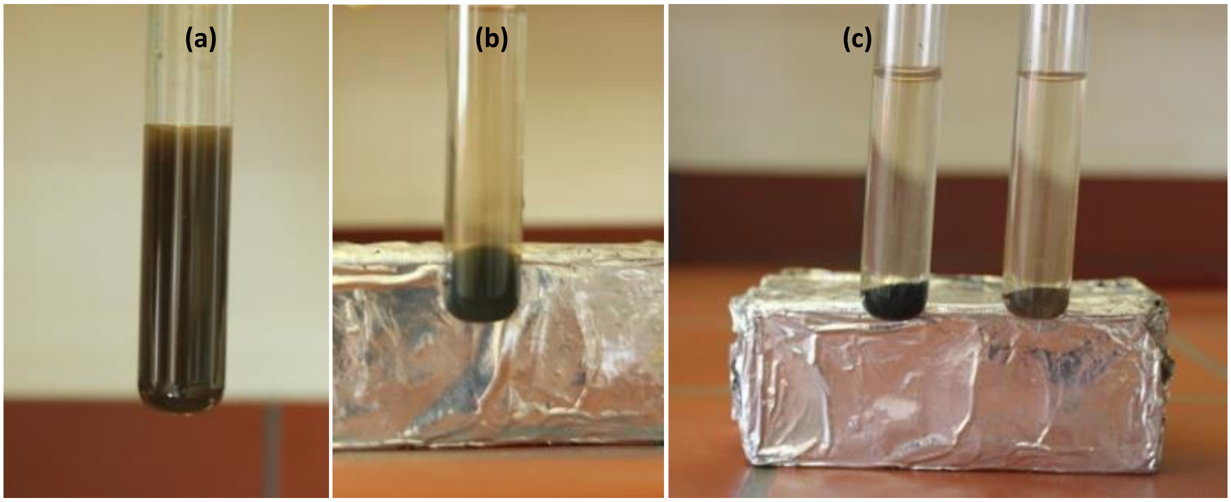

Figure 6. (a) Fe_3O_4 MNPs dispersion in water,(b) separation of the same MNPs by an external magnet, (c) Fe_3O_4 MNPs (left) and AMNPs (right) separation by an external magnet

Brunauer–Emmett–Teller (BET) surface areas of the nanoparticles were determined by N_2 adsorption/desorption, the measured surface area (m^2/g) for SMNPs, AMNPs and β-CD MNPs are 63.1, 48.6 and 29 (m^2/g) respectively while the mean pore diameter (nm) are 13.6, 17.8 and 30.4 respectively.

Scanning electron microscopy (SEM) and transmission electron microscopy (TEM) images of synthesized Fe_3O_4 magnetic nanoparticles are shown in Figures 7 and 8 respectively. SEM images in 500 nm and 2μm magnitudes show bulk and amorphous shape of MNPs. TEM images exhibit the fact that the MNPs are well dispersed measuring about 20 nm. The dark and non-spherical parts of the TEM images could be an indication of the aggregation of MNPs.

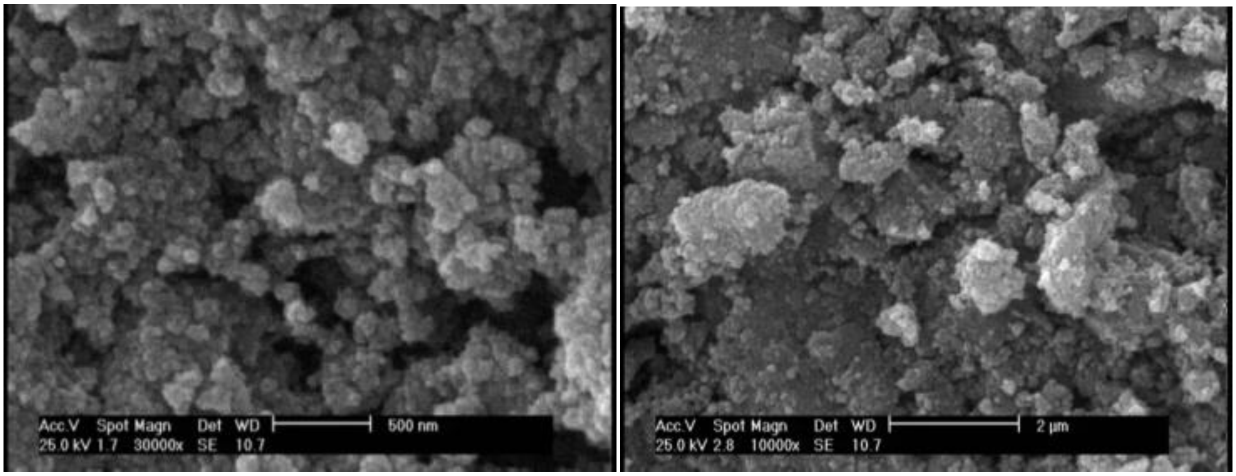

Figure 7. SEM images of Fe_3O_4 MNPs in 500 nm (left) and 2µm (right) magnitudes

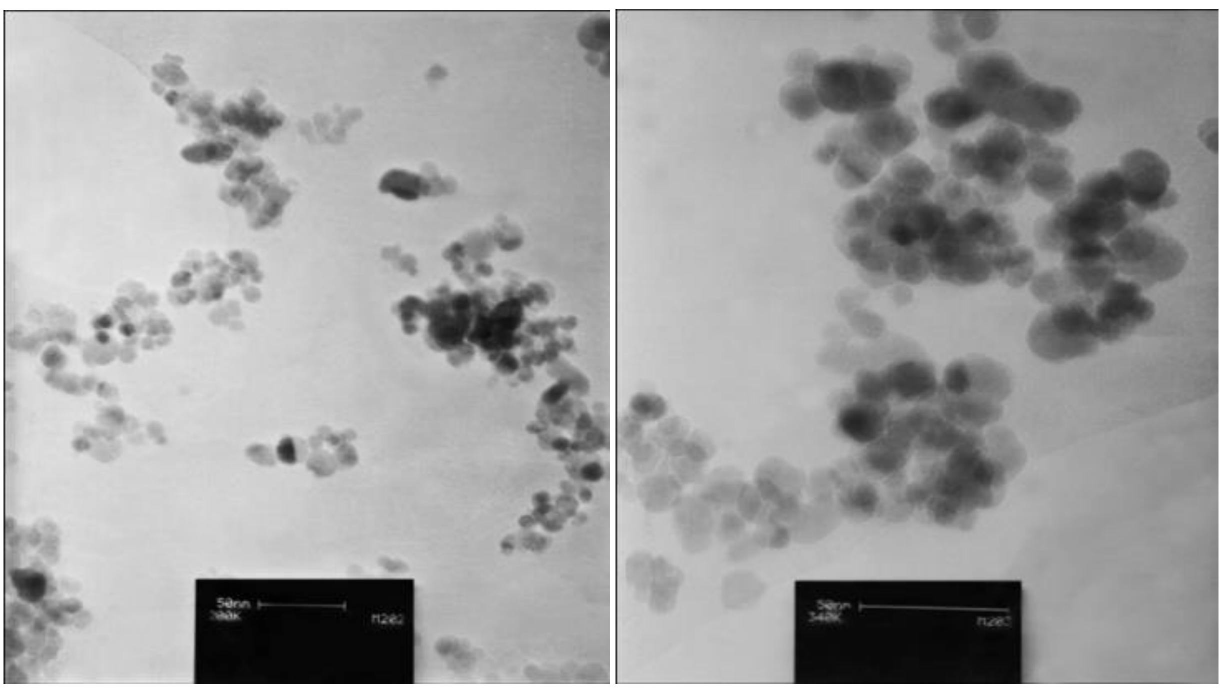

Figure 8. TEM images of Fe_3O_4 MNPs in 50 nm magnitudes

3.2. Adsorption of Lead (II) and Copper (II) ions by CD-MNPs

Lead (II) and Copper (II) ion adsorption experiments were carried out using batch equilibrium technique in aqueous solutions at pH ranging 2 - 6 at temperatures ranging between 25–55 °C. About 50 mg of magnetic nano adsorbents were added to 10 mL of Pb^{2+} and Cu^{2+} solution of various concentrations and shaken to reach the equilibrium. After attaining equilibrium, magnetic nano adsorbents were removed using a permanent magnet and the supernatant was collected to measure the metal ion concentration. For kinetic experiments, initial metal ion concentrations used was 50 mg L^{-1} and the pH maintained at 6. At different time intervals the adsorbent was removed by magnetic decantation and metal ions concentrations were measured. The amount of metal ions adsorbed onto β-CD-MNPs (q_e) and removal efficiency (R) were calculated using the following equations (1-2):

$$q_e = \frac{(C_0 - C_f)}{m} V \quad (1)$$

$$R = \left(\frac{C_0 - C_f}{C_f}\right) \times 100 \quad (2)$$

Where, V (L) is the volume, C_0 and C_e (mg L^{-1}) are the initial and final solution concentration of metal ions respectively, and m (g) is the dry mass of the solid.

3.2.1 Effect of pH on adsorption

Owing to the fact that in an aqueous solution, Copper (II) ions can exist not only as Cu^{2+} but also in the form of $Cu(OH)^+$, $Cu(OH)_2$,$Cu(OH)_3$ and $Cu(OH)_4^{2-}$. At pH>6 precipitation of $Cu(OH)_2$

also occurs and evaluation of the effect of pH was conducted in pH ranging from 2 to 6. In order to obtain desired solutions, copper (II) nitrate trihydrate and Lead (II) nitrate salts were dissolved in 0.1 molar nitrate buffer (for pH= 2-3) and 0.1 molar acetate buffer (for pH=4-6). As shown in Fig. 9, an increase in pH resulted in the gradual increase in metal ion adsorption.[61] Therefore, pH=6 was selected as the optimum pH and all tests were performed at this pH.

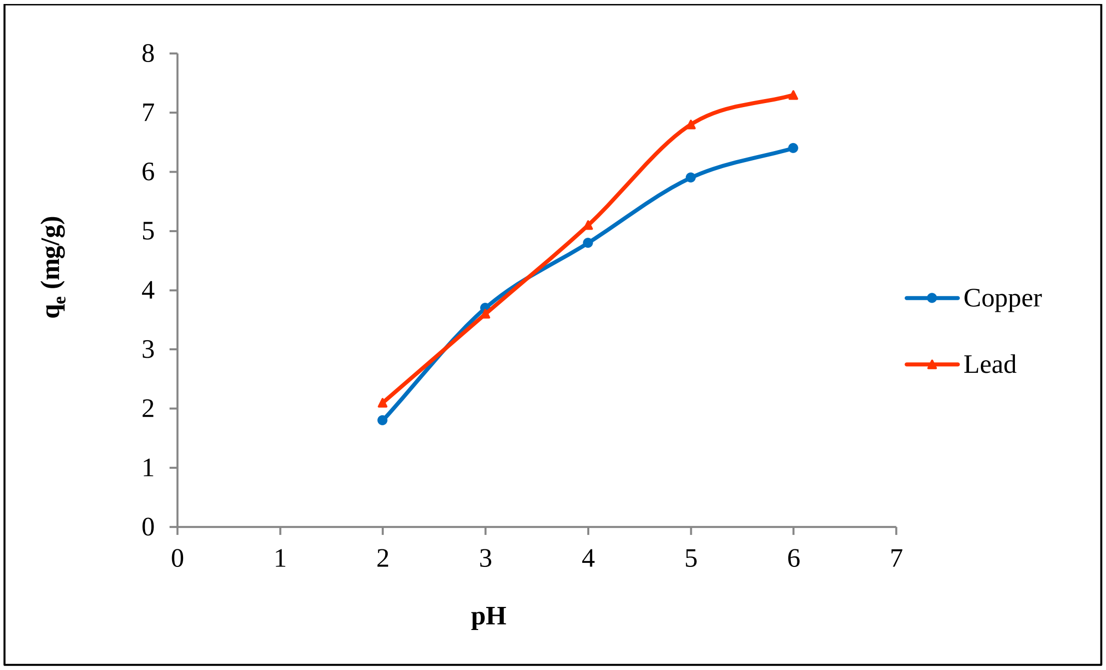

Figure 9. The effect of pH on adsorption of Copper (II) and Lead (II) ions

3.2.2 Effect of contact time and adsorption kinetics

The kinetics of adsorption was investigated to better comprehend the adsorption process. The effect of contact time on adsorption of Lead (II) and Copper (II) ions on β-CD-MNPs at different temperatures are shown in Figures 10 and 11 respectively. A high rate of adsorption of metal ions can be observed at the beginning. At 25 °C, 36% of Copper (II) ion and 37% of the Lead (II) ion adsorption is achieved within 5 minutes and equilibrium is attained approximately 30 minutes later.

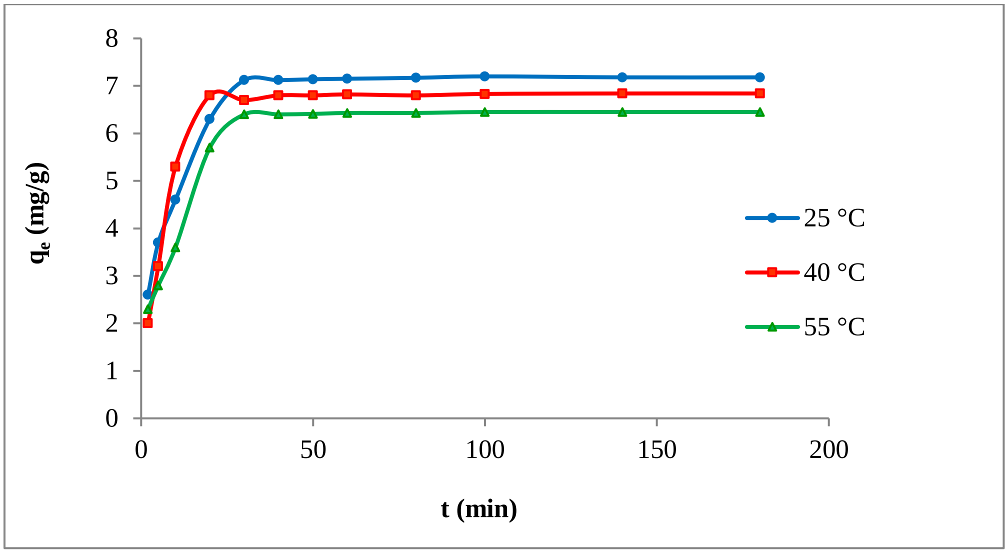

Figure 10. The effect of contact time on adsorption of Lead (II) ions at different temperatures

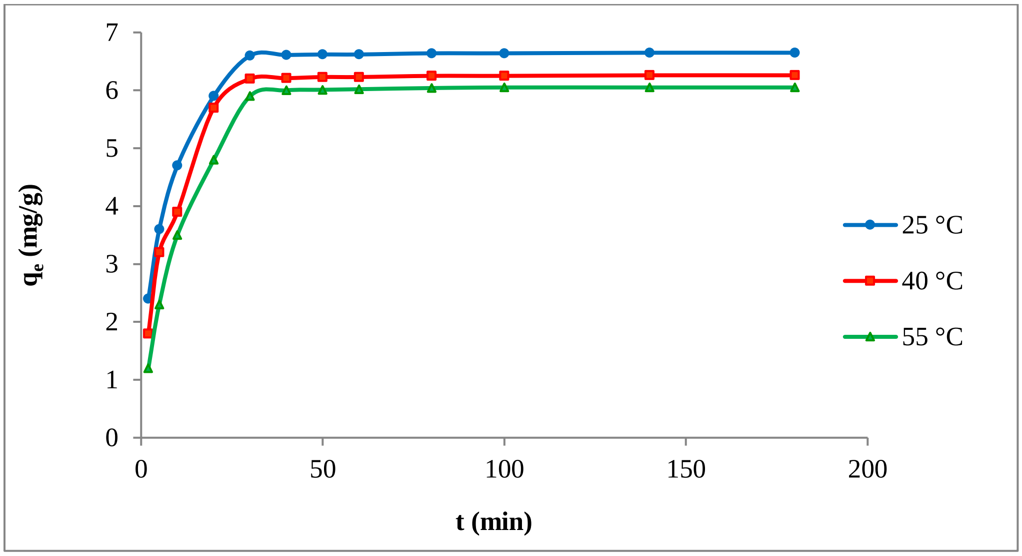

Figure 11 The effect of contact time on adsorption of Copper (II) ions at different temperatures

3.2.3 Adsorption kinetics of Copper (II) and Lead (II) ions removal by β-CD-MNPs

In order to study the adsorption process, kinetic models are used to corroborate experimental data. The adsorption data of Copper (II) and Lead (II) ions at different time intervals are fitted to pseudo second order (Figures 12 and 13) and pseudo first order kinetic model. The pseudo first order kinetic model is expressed as follows (equation 3):

$$\log\left(q_e - q_t\right) = \log\left(q_e\right) - \frac{k}{2.303}t \qquad (3)$$

q_e and q_t (mg/g) are adsorption capacities of metal ions at equilibrium at any time, t (min) respectively, the rate constant of pseudo first order adsorption k (min^{-1}) is determined by the slope of log(q_e - q_t) versus t. The pseudo second order model is expressed by equation (4):

$$\frac{t}{q_t} = \frac{1}{k_2 q_e^{\ 2}} + \frac{1}{q_e}t \qquad (4)$$

Where, k_2 is the equilibrium rate constant for pseudo second order adsorption (g mg^{-1} min^{-1}) which is obtained by the slope and intercept of the plot of t/q_t versus t. q_e and q_t (mg/g) refer to the adsorption capacity of metal ions at equilibrium and at any time, t (min) respectively.

Pseudo first order and pseudo second order kinetic parameters for Lead (II) and Copper (II) are listed in tables 1 and 2 respectively. As it can be seen, the adsorbent system can be well described by pseudo second order kinetic is confirmed by higher correlation coefficient (R^2) for pseudo second order kinetic model and q_e values obtained from pseudo second order kinetic model rather than those obtained from pseudo first order model are more consistent with the experimental q_e values. So far, many other adsorbents have been reported to be more consistent with the pseudo second order kinetic model.[62]

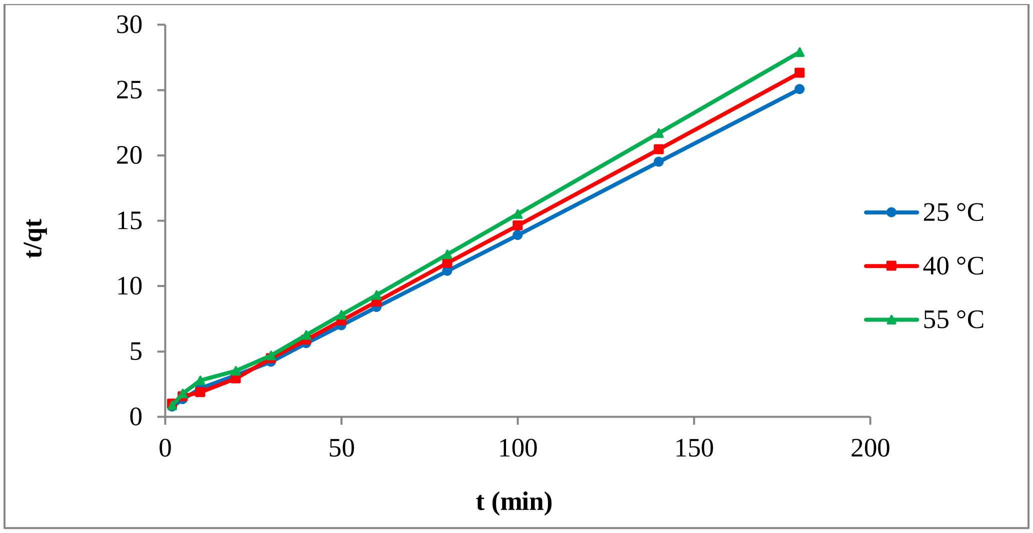

Figure 12 Pseudo second order kinetics for adsorption of Pb(II) ions (pH= 6)

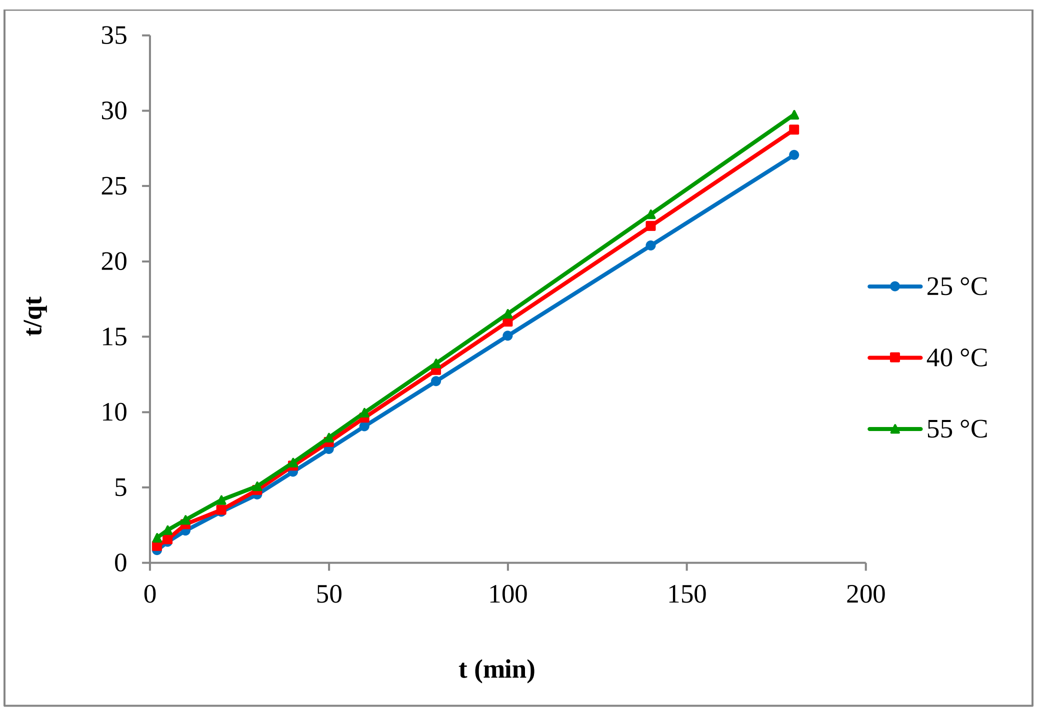

Figure 13. Pseudo second order kinetics for adsorption of Cu (II) ions (pH= 6)

Table 1 Adsorption kinetic parameters of Lead (II) ions onto β-CD-MNPs

Temperature	**pseudo first order kinetic**			**pseudo second order kinetic**		
	$k_1(min^{-1})$	$q_e(mg/g)$	R^2	$k_2g/(mg.min)$	$q_e(mg/g)$	R^2
25°C	0.084	3.583	0.8989	0.0445	7.364	0.9992
40°C	0.0569	1.287	0.6880	0.0541	6.993	0.9991
55°C	0.0797	3.083	0.8402	0.0395	6.657	0.9984

Table 2 Adsorption kinetic parameters of Copper (II) ions onto β-CD-MNPs

Temperature	**pseudo first order kinetic**			**pseudo second order kinetic**		
	$k_1(min^{-1})$	$q_e(mg/g)$	R^2	$k_2g/(mg.min)$	$q_e(mg/g)$	R^2
25°C	0.0666	1.997	0.8284	0.0553	6.798	0.9995
40°C	0.067	2.099	0.8435	0.0471	6.435	0.999
55°C	0.086	4.393	0.9338	0.0293	6.325	0.9978

3.2.4 Adsorption isotherm of Copper (II) and Lead (II) ions

The adsorption isotherms of Copper (II) and Lead (II) ions were studied using the Langmuir and Freundlich models. The Langmuir isotherm assumes monolayer adsorption on a uniform surface with a finite number of adsorption sites. Once a site is filled, no further sorption can take place at that site and the surface will eventually reach a saturation point where the maximum adsorption of the surface will be achieved.[63] The Langmuir equation is expressed as follows:

$$\frac{C_e}{q_e} = \frac{C_e}{q_m} + \frac{1}{q_m K_L} \qquad (5)$$

Where, C_e is the equilibrium concentration in solution (mg/L), q_e is the amount of adsorbed material at equilibrium (mg/g), q_m the maximum capacity of adsorbent (mg/g), and K_L the Langmuir constant (L/mg). The Freundlich isotherm is applicable to both monolayer (chemisorption) and multilayer adsorption (physisorption) and is based on the assumption that the adsorbate adsorbs onto the heterogeneous surface of an adsorbent. The Freundlich equation is expressed as follows:

$$\ln q_e = \frac{1}{n} \ln C_e + \ln K_f \qquad (6)$$

Where, K_F is Freundlich constant (L/mg), n is the heterogeneity factor, q_e is the amount of adsorbed material at equilibrium (mg/g)and C_e is the equilibrium concentration in solution (mg/L). The slope and intercept of the linear plot of C_e/q_e versus C_e can be used to obtain q_m and K_L values of the Langmuir equation. K_F and 1/n values in the Freundlich equation can also be determined from slope and intercept of linear plot of ln q_e versus ln C_e. In almost all experiments correlation coefficient (R^2) values for Langmuir equation are higher than Freundlich equation and Langmuir isotherms show better fit to experimental data (Figures 14 and 15), suggesting that Copper (II) and Lead (II) ion adsorption on β-CD-MNPs is of monolayer coverage.

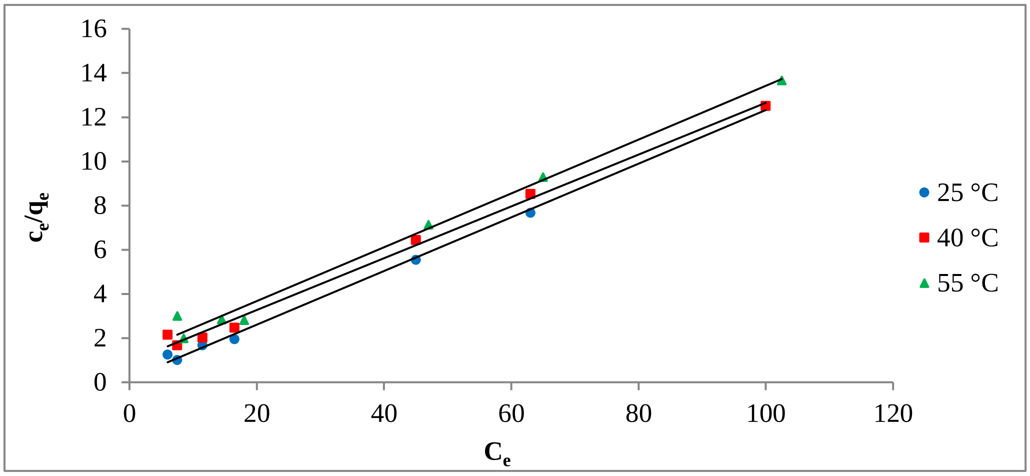

Figure 14. The Langmuir isotherm plots for Lead (II) ions adsorption by CD-MNPs at pH=6

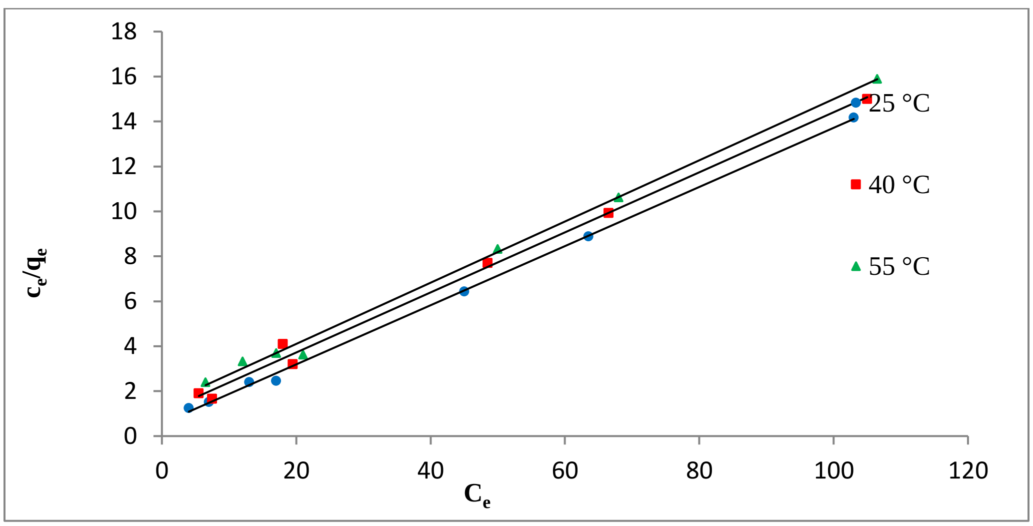

Figure 15. The Langmuir isotherm plots for Copper (II) ions adsorption by β-CD-MNPs at pH=6

The Freundlich isotherms for Lead (II) and Copper (II) ion adsorption at different temperatures (25, 40 and 55°C)are given in Figures 16 and 17 respectively.

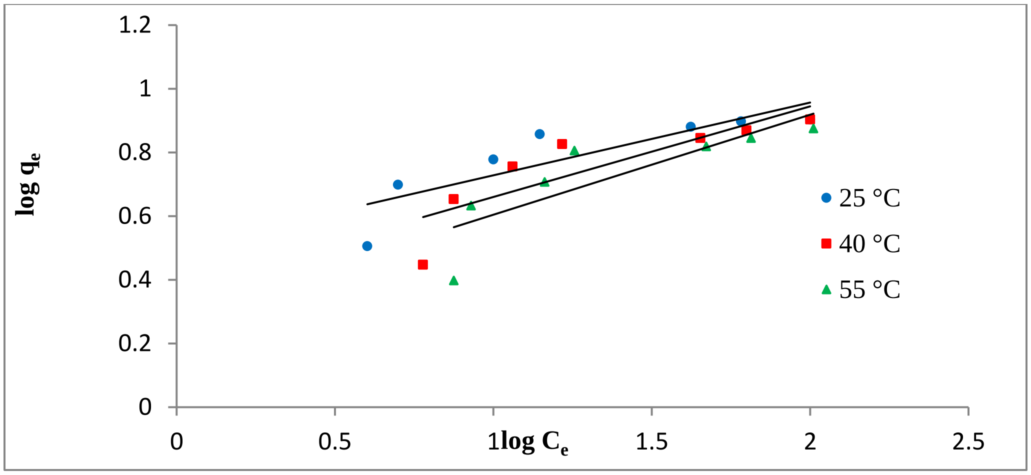

Figure 16. Freundlich isotherm for Lead (II) ions adsorption by β-CD-MNPs at pH=6

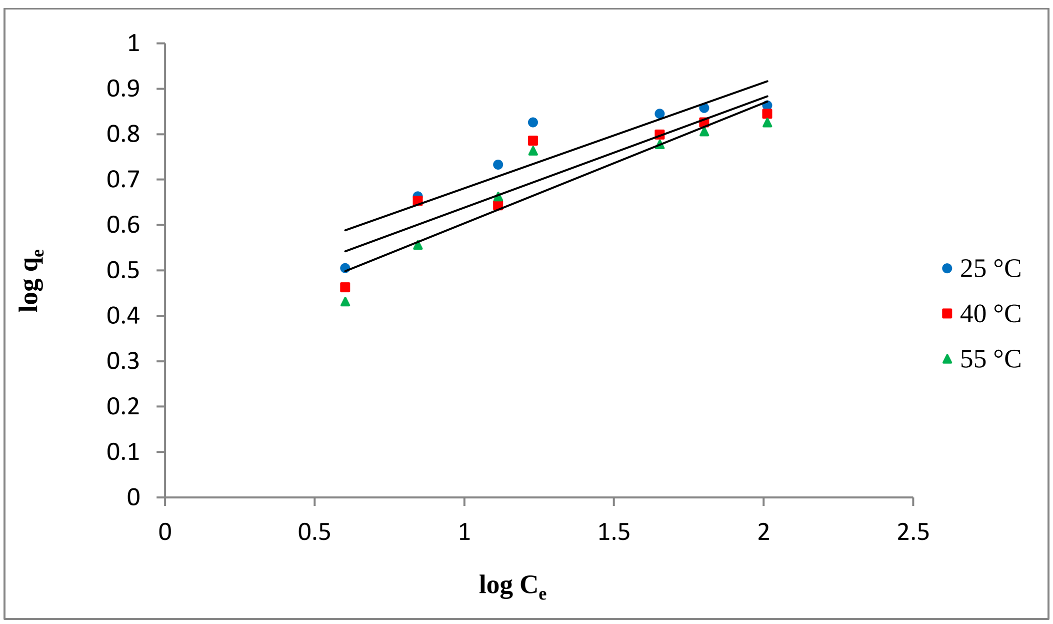

Figure 17. Freundlich isotherm for Copper (II) ions adsorption by β-CD-MNPs at pH=6

The adsorption isotherm parameters for Lead (II) ion adsorption on the β-CD MNPs are given in Table 4 and those for Copper (II) are given in Table 5.

Table 3 Adsorption isotherm parameters for Lead (II) ions adsorption on β-CD-MNPs at pH=6

Temperature	Langmuir isotherm constants			Freundlich isotherm constants		
	k (L/mg)	q_m (mg/g)	R^2	k_f (mg/g)(L/mg)	N	R^2
25°C	0.2492	8.354	0.9987	3.160	4.376	0.7337
40°C	0.1270	8.525	0.9941	2.374	3.513	0.7238
55°C	0.0985	8.210	0.9891	1.951	3.183	0.6993

Table 4 Adsorption isotherm parameters for Copper (II) ions adsorption on β-CD-MNPs at pH=6

Temperature	Langmuir isotherm constants			Freundlich isotherm constants		
	k (L/mg)	q_m (mg/g)	R^2	k_f (mg/g)(L/mg)	N	R^2
25°C	0.235	7.599	0.9988	2.806	4.297	0.819
40°C	0.127	7.485	0.9945	2.310	3.924	0.790
55°C	0.098	7.342	0.9965	1.760	3.222	0.844

The standard Gibbs free energy ΔG^0 (kJ mol^{-1}), standard enthalpy change ΔH^0 (kJ mol^{-1}), and standard entropy change ΔS^0 (J mol^{-1} K^{-1}) were calculated using the following equations (7-8):

$$\ln K_0 = -\frac{\Delta H^0}{RT} + \frac{\Delta S^0}{R} \quad (7)$$

$$\Delta G^0 = -RT\ln K_0 \quad (8)$$

$$(9) K_0 = C_{solid} / C_{liquid}$$

Where, T is the temperature in Kelvin, R the gas constant (8.314 J. mol^{-1} K^{-1}), C_{solid} the amount of ions adsorbed by CD-MNPs at equilibrium and $C_{liquid}$the equilibrium concentration of ions in solution. $\Delta S^0$and ΔH^0 values can also be determined from the slope and intercept of the plot of *Ln* K^0versus *1/T*, respectively (Fig 18 and table 5). The Gibbs free energy (ΔG^0) indicates the degree of spontaneity of the adsorption process and the low values reflect an energetically favorable adsorption process. The negative value of ΔH^0confirms that the sorption process was exothermic in nature and a given amount of heat is evolved during the binding of ions onto the surface of adsorbent. The highly negative ΔS^0 values indicate significant decrease in the degree of randomness at solid/liquid interface during the sorption process.[64]

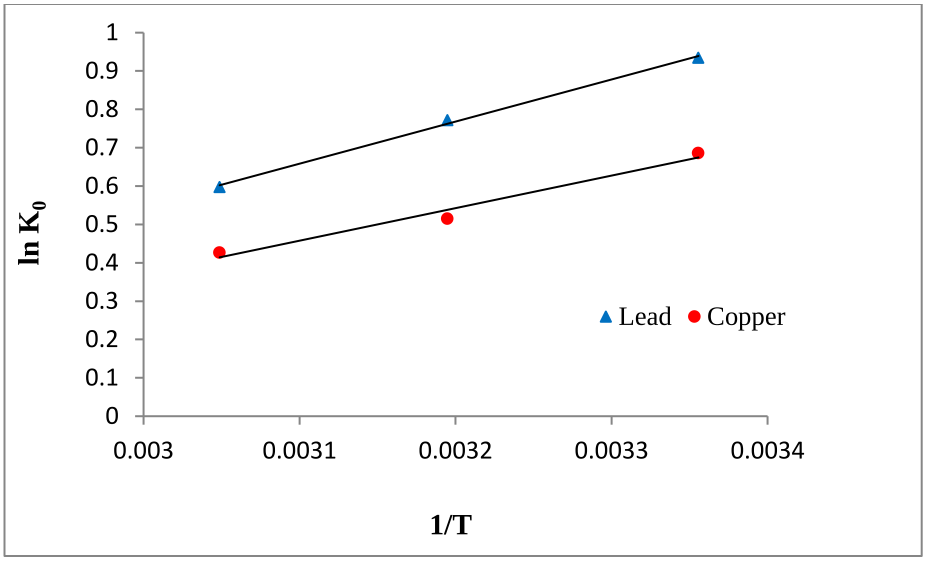

Figure 18. Determination of thermodynamic parameters for the sorption of Lead (II) and Copper (II) ions onto β-CD-MNPs

Table 5 Thermodynamic parameters for the adsorption of Lead (II) and Copper (II) ions onto CD-MNPs

Metal	R^2	ΔH^0(kJ/mol)	ΔS^0(J/k.mol)	ΔG^0(kJ/mol)		
				298 K	313 K	328 K
Lead	0.9976	-9.127	-22.819	-2.315	-2.009	-1.628
Copper	0.9769	-7.054	-18.062	-1.698	-1.340	-1.165

3.3 Regeneration of nanoparticles

The regeneration of adsorbents is a crucial aspect for academic research and indusrril implementation.[65] The effect of pH on the adsorption of Lead (II) and Copper (II) ions revealed that the minimum adsorption of both metal ions occurred at low pH (pH=2). Furthermore, ion desorption experiments in many reports have confirmed that different acids could be favorable candidates for the desorption of adsorbed metal ions[66]and it is believed that the bonding between the active sites of magnetic nanoadsorbents and metal ions is not sufficiently strong in acidic conditions. In order to assume the possibility of recycling β-CD-MNPs adsorbent, desorption of Lead (II) and Copper (II) ions was conducted using 0.1(M) citric acid as an eluent. The regeneration studies suggest that the β-CD-MNPs can be used efficiently in 4 runs with negligible loss of adsorption capability of both ions (Fig. 19).

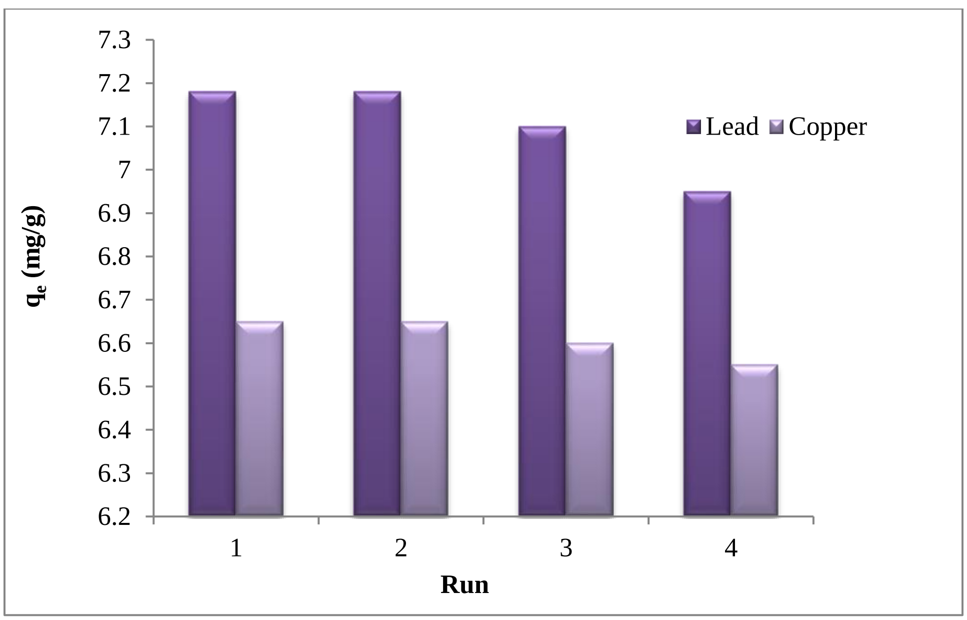

Figure 19. Regeneration of CD-MNPs

4. Conclusion

Superparamagnetic silica coated Fe_3O_4 magnetic nanoparticles were prepared and functionalized with APTES and β–CD-OTS and these nanoparticles were then used as adsorbents for the removal of Lead (II) and Copper (II) ions from aqueous solutions. Grafted β–CD provides numerous surface hydroxyl and carbonyl groups, which facilitate metal ion removal. Different factors such as pH, temperature and adsorbent dosage can affect the adsorption process. Batch adsorption experiments revealed that in a range of pH=2-6, pH=6 can be chosen as the optimum pH. The kinetics of adsorption was observed to follow pseudo-second order and equilibrium is reached in approximately 30 minutes. The equilibrium data are well fitted to Langmuir isotherm. The effect of contact time at different temperatures confirms that an increase in temperature results in a gradual decrease of metal ions uptake. Determination thermodynamic parameters revealed that ΔH^0values for both Lead (II) and Copper (II) ions are negative, which confirm the exothermic nature of the sorption process. In addition, the adsorbed ions could be desorbed effectively from β-CD-MNPs surface by citric acid and could be employed as a reusable adsorbent and would be an economically viable option.

Acknowledgements

The authors acknowledge the Institute for Advanced Studies in Basic Sciences (IASBS), Iran for financial support.

References

1. Duruibe JO, Ogwuegbu M, Egwurugwu J. Heavy metal pollution and human biotoxic effects. *International Journal of physical sciences* 2007, 2:112-118.
2. Sorensen EM. *Metal poisoning in fish*: CRC press; 1991.
3. Kampalanonwat P, Supaphol P. Preparation and Adsorption Behavior of Aminated Electrospun Polyacrylonitrile Nanofiber Mats for Heavy Metal Ion Removal. *ACS Applied Materials & Interfaces* 2010, 2:3619-3627.

4. Daochalermwong A, Chanka N, Songsrirote K, Dittanet P, Niamnuy C, Seubsai A. Removal of Heavy Metal Ions Using Modified Celluloses Prepared from Pineapple Leaf Fiber. *ACS Omega* 2020, 5:5285-5296.
5. Dąbrowski A, Hubicki Z, Podkościelny P, Robens E. Selective removal of the heavy metal ions from waters and industrial wastewaters by ion-exchange method. *Chemosphere* 2004, 56:91-106.
6. Hubicki Z, Kołodyńska D. Selective removal of heavy metal ions from waters and waste waters using ion exchange methods. *Ion exchange technologies* 2012:193-240.
7. Cortina J, Miralles N. Kinetic studies on heavy metal ions removal by impregnated resins containing di-(2, 4, 4-trymethylpentyl) phosphinic acid. *Solvent extraction and ion exchange* 1997, 15:1067-1083.
8. Mercier L, Pinnavaia TJ. Heavy metal ion adsorbents formed by the grafting of a thiol functionality to mesoporous silica molecular sieves: factors affecting Hg (II) uptake. *Environmental Science & Technology* 1998, 32:2749-2754.
9. Ozaki H, Sharma K, Saktaywin W. Performance of an ultra-low-pressure reverse osmosis membrane (ULPROM) for separating heavy metal: effects of interference parameters. *Desalination* 2002, 144:287-294.
10. Herrmann J-M. Heterogeneous photocatalysis: fundamentals and applications to the removal of various types of aqueous pollutants. *Catalysis today* 1999, 53:115-129.
11. Sis H, Uysal T. Removal of heavy metal ions from aqueous medium using Kuluncak (Malatya) vermiculites and effect of precipitation on removal. *Applied Clay Science* 2014, 95:1-8.
12. Tran T-K, Chiu K-F, Lin C-Y, Leu H-J. Electrochemical treatment of wastewater: Selectivity of the heavy metals removal process. *International Journal of hydrogen energy* 2017, 42:27741-27748.
13. Tomalia DA. In quest of a systematic framework for unifying and defining nanoscience. *Journal of Nanoparticle Research* 2009, 11:1251-1310.
14. Hartland GV. Measurements of the material properties of metal nanoparticles by time-resolved spectroscopy. *Physical Chemistry Chemical Physics* 2004, 6:5263-5274.
15. Guisbiers G, Mejía-Rosales S, Leonard Deepak F. Nanomaterial Properties: Size and Shape Dependencies. *Journal of Nanomaterials* 2012, 2012:180976.
16. Chauhan VP, Jain RK. Strategies for advancing cancer nanomedicine. *Nat Mater* 2013, 12:958-962.
17. Ray P, Haideri N, Haque I, Mohammed O, Chakraborty S, Banerjee S, Quadir M, Brinker AE, Banerjee SK. The Impact of Nanoparticles on the Immune System: A Gray Zone of Nanomedicine. *Journal of Immunological Sciences* 2021, 5.
18. Ray P, Dutta D, Haque I, Nair G, Mohammed J, Parmer M, Kale N, Orr M, Jain P, Banerjee S, et al. pH-Sensitive Nanodrug Carriers for Codelivery of ERK Inhibitor and Gemcitabine Enhance the Inhibition of Tumor Growth in Pancreatic Cancer. *Molecular Pharmaceutics* 2021, 18:87-100.
19. Ray P, Kale N, Quadir M. New side chain design for pH-responsive block copolymers for drug delivery. *Colloids and Surfaces B: Biointerfaces* 2021, 200:111563.
20. Abdullah CS, Ray P, Alam S, Kale N, Aishwarya R, Morshed M, Dutta D, Hudziak C, Banerjee SK, Mallik S, et al. Chemical Architecture of Block Copolymers Differentially Abrogate Cardiotoxicity and Maintain the Anticancer Efficacy of Doxorubicin. *Molecular Pharmaceutics* 2020, 17:4676-4690.
21. Confeld MI, Mamnoon B, Feng L, Jensen-Smith H, Ray P, Froberg J, Kim J, Hollingsworth MA, Quadir M, Choi Y, et al. Targeting the tumor core: hypoxia-responsive nanoparticles for delivery of chemotherapy to pancreatic tumors. *Molecular Pharmaceutics* 2020.
22. Sarker NC, Ray P, Pfau C, Kalavacharla V, Hossain K, Quadir M. Development of Functional Nanomaterials from Wheat Bran Derived Arabinoxylan for Nucleic Acid Delivery. *Journal of Agricultural and Food Chemistry* 2020, 68:4367-4373.
23. Ray P, Nair G, Ghosh A, Banerjee S, Golovko MY, Banerjee SK, Reindl KM, Mallik S, Quadir M. Microenvironment-sensing, nanocarrier-mediated delivery of combination chemotherapy for pancreatic cancer. *Journal of Cell Communication and Signaling* 2019.
24. Ray P, Alhalhooly L, Ghosh A, Choi Y, Banerjee S, Mallik S, Banerjee S, Quadir M. Size-Transformable, Multifunctional Nanoparticles from Hyperbranched Polymers for Environment-Specific Therapeutic Delivery. *ACS Biomaterials Science & Engineering* 2019, 5:1354-1365.
25. Ghosh A, Sarkar S, Ghosh S, Ray P, Quadir M, Banerjee SK, Banerjee S. Abstract 1234: Zoledronic acid-induced suppression of invasive phenotypes of pancreatic cancer cells is mediated through downregulation of CYR61/CCN1. *Cancer Research* 2019, 79:1234.
26. Ray P, Ferraro M, Haag R, Quadir M. Dendritic Polyglycerol-Derived Nano-Architectures as Delivery Platforms of Gemcitabine for Pancreatic Cancer. *Macromol Biosci* 2019, 19:e1900073.
27. Ray P, Confeld M, Borowicz P, Wang T, Mallik S, Quadir M. PEG-b-poly (carbonate)-derived nanocarrier platform with pH-responsive properties for pancreatic cancer combination therapy. *Colloids Surf B Biointerfaces* 2018, 174:126-135.
28. Ray P, Gidley D, Badding JV, Lueking AD. UV and chemical modifications of polymer of Intrinsic Microporosity 1 to develop vibrational spectroscopic probes of surface chemistry and porosity. *Microporous and Mesoporous Materials* 2019, 277:29-35.
29. Ray JK, Singha R, Ray D, Ray P, Rao DY, Anoop A. Palladium-catalyzed expedient Heck annulations in 1-bromo-1,5-dien-3-ols: Exceptional formation of fused bicycles. *Tetrahedron Letters* 2019, 60:931-935.

30. Ray P, Xu E, Crespi VH, Badding JV, Lueking AD. In situ vibrational spectroscopy of adsorbed nitrogen in porous carbon materials. *Physical Chemistry Chemical Physics* 2018, 20:15411-15418.
31. Ray JK, Paul S, Ray P, Singha R, Rao DY, Nandi S, Anoop A. Pd-catalyzed intramolecular sequential Heck cyclization and oxidation reactions: a facile pathway for the synthesis of substituted cycloheptenone evaluated using computational studies. *New Journal of Chemistry* 2017, 41:278-284.
32. Chaudhuri S, Maity S, Roy M, Ray P, Ray JK. A Vinyl Radical Cyclization Route to Hydroxycyclohexene Fused Carbocycles. *Asian Journal of Chemistry* 2016, 28.
33. Ray P, Gray JL, Badding JV, Lueking AD. High-Pressure Reactivity of Triptycene Probed by Raman Spectroscopy. *The Journal of Physical Chemistry B* 2016, 120:11035-11042.
34. Ray P. Interactions of nitrogen and hydrogen with various 1D and 3D carbon materials probed via in-situ vibrational spectroscopy. *Ph. D. Thesis* 2016.
35. Wang C-Y, Ray P, Gong Q, Zhao Y, Li J, Lueking AD. Influence of gas packing and orientation on FTIR activity for CO chemisorption to the Cu paddlewheel. *Physical Chemistry Chemical Physics* 2015, 17:26766-26776.
36. Brahma S, Ray P, Singha R, Ray JK. Visible Colourimetric and Ratiometric Fluorescent Chemosensors for Cu (II) and Ni (II) Ions. *Asian Journal of Chemistry* 2016, 28:1035.
37. Singha R, Roy S, Nandi S, Ray P, Ray JK. Palladium-catalyzed one-pot Suzuki–Miyaura cross coupling followed by oxidative lactonization: a novel and efficient route for the one-pot synthesis of benzo[c]chromene-6-ones. *Tetrahedron Letters* 2013, 54:657-660.
38. Ray D, Nasima Y, Sajal MK, Ray P, Urinda S, Anoop A, Ray JK. Palladium-Catalyzed Intramolecular Oxidative Heck Cyclization and Its Application toward a Synthesis of (±)-β-Cuparenone Derivatives Supported by Computational Studies. *Synthesis* 2013, 45:1261-1269.
39. Ray J, Bhowmik L. Preparation and Evaluation of Novel Bamboo-Polymer Composites. 2021.
40. Bee TG, McCarthy TJ. Surface modification of poly (chlorotrifluoroethylene): introduction of reactive carboxylic acid functionality. *Macromolecules* 1992, 25:2093-2098.
41. Khire VS, Lee TY, Bowman CN. Surface modification using thiol− acrylate conjugate addition reactions. *Macromolecules* 2007, 40:5669-5677.
42. Garg M, Tak BR, Rao VR, Singh R. Giant UV photoresponse of GaN-based photodetectors by surface modification using phenol-functionalized porphyrin organic molecules. *ACS applied materials & interfaces* 2019, 11:12017-12026.
43. Bourlinos AB, Gournis D, Petridis D, Szabó T, Szeri A, Dékány I. Graphite oxide: chemical reduction to graphite and surface modification with primary aliphatic amines and amino acids. *Langmuir* 2003, 19:6050-6055.
44. Jo S, Park K. Surface modification using silanated poly (ethylene glycol) s. *Biomaterials* 2000, 21:605-616.
45. Popat KC, Mor G, Grimes CA, Desai TA. Surface modification of nanoporous alumina surfaces with poly (ethylene glycol). *Langmuir* 2004, 20:8035-8041.
46. Bruce IJ, Sen T. Surface modification of magnetic nanoparticles with alkoxysilanes and their application in magnetic bioseparations. *Langmuir* 2005, 21:7029-7035.
47. Jain TK, Roy I, De TK, Maitra A. Nanometer Silica Particles Encapsulating Active Compounds: A Novel Ceramic Drug Carrier. *Journal of the American Chemical Society* 1998, 120:11092-11095.
48. Clément M, Abdellah I, Ray P, Martini C, Coppel Y, Remita H, Lampre I, Huc V. Synthesis and NMR study of trimethylphosphine gold(i)-appended calix[8]arenes as precursors of gold nanoparticles. *Inorganic Chemistry Frontiers* 2020.
49. Ray P, Clément M, Martini C, Abdellah I, Beaunier P, Rodriguez-Lopez J-L, Huc V, Remita H, Lampre I. Stabilisation of small mono- and bimetallic gold–silver nanoparticles using calix[8]arene derivatives. *New Journal of Chemistry* 2018, 42:14128-14137.
50. André E, Boutonnet B, Charles P, Martini C, Aguiar-Hualde JM, Latil S, Guérineau V, Hammad K, Ray P, Guillot R, et al. A New, Simple and Versatile Strategy for the Synthesis of Short Segments of Zigzag-Type Carbon Nanotubes. *Chemistry* 2016, 22:3105-3114.
51. Oroujeni M, Kaboudin B, Xia W, Jönsson P, Ossipov DA. Conjugation of cyclodextrin to magnetic Fe3O4 nanoparticles via polydopamine coating for drug delivery. *Progress in Organic Coatings* 2018, 114:154-161.
52. Mrówczyński R, Jędrzak A, Szutkowski K, Grześkowiak BF, Coy E, Markiewicz R, Jesionowski T, Jurga S. Cyclodextrin-based magnetic nanoparticles for cancer therapy. *Nanomaterials* 2018, 8:170.
53. Lee S-F, Zhu X-M, Wang Y-XJ, Xuan S-H, You Q, Chan W-H, Wong C-H, Wang F, Yu JC, Cheng CH. Ultrasound, pH, and magnetically responsive crown-ether-coated core/shell nanoparticles as drug encapsulation and release systems. *ACS applied materials & interfaces* 2013, 5:1566-1574.
54. Ghosh S, Badruddoza AZM, Uddin MS, Hidajat K. Adsorption of chiral aromatic amino acids onto carboxymethyl-β-cyclodextrin bonded Fe3O4/SiO2 core–shell nanoparticles. *Journal of Colloid and Interface Science* 2011, 354:483-492.
55. Sun Y-k, Ma M, Zhang Y, Gu N. Synthesis of nanometer-size maghemite particles from magnetite. *Colloids and Surfaces A: Physicochemical and Engineering Aspects* 2004, 245:15-19.

56. Kobayashi M, Juillerat F, Galletto P, Bowen P, Borkovec M. Aggregation and Charging of Colloidal Silica Particles: Effect of Particle Size. *Langmuir* 2005, 21:5761-5769.
57. Tang W, Ng SC. Synthesis of cationic single-isomer cyclodextrins for the chiral separation of amino acids and anionic pharmaceuticals. *Nat Protoc* 2007, 2:3195-3200.
58. Belyakova LA, Kazdobin KA, Belyakov VN, Ryabov SV, Danil de Namor AF. Synthesis and properties of supramolecular systems based on silica. *Journal of Colloid and Interface Science* 2005, 283:488-494.
59. Ji Y, Liu X, Guan M, Zhao C, Huang H, Zhang H, Wang C. Preparation of functionalized magnetic nanoparticulate sorbents for rapid extraction of biphenolic pollutants from environmental samples. *Journal of Separation Science* 2009, 32:2139-2145.
60. Banerjee SS, Chen D-H. Magnetic Nanoparticles Grafted with Cyclodextrin for Hydrophobic Drug Delivery. *Chemistry of Materials* 2007, 19:6345-6349.
61. Shamim N, Hong L, Hidajat K, Uddin MS. Thermosensitive polymer (N-isopropylacrylamide) coated nanomagnetic particles: preparation and characterization. *Colloids Surf B Biointerfaces* 2007, 55:51-58.
62. Zhou Y-T, Branford-White C, Nie H-L, Zhu L-M. Adsorption mechanism of Cu2+ from aqueous solution by chitosan-coated magnetic nanoparticles modified with α-ketoglutaric acid. *Colloids and Surfaces B: Biointerfaces* 2009, 74:244-252.
63. Kamari A, Ngah WSW. Isotherm, kinetic and thermodynamic studies of lead and copper uptake by H2SO4 modified chitosan. *Colloids and Surfaces B: Biointerfaces* 2009, 73:257-266.
64. Boparai HK, Joseph M, O'Carroll DM. Kinetics and thermodynamics of cadmium ion removal by adsorption onto nano zerovalent iron particles. *J Hazard Mater* 2011, 186:458-465.
65. Sheng G, Wang S, Hu J, Lu Y, Li J, Dong Y, Wang X. Adsorption of Pb(II) on diatomite as affected via aqueous solution chemistry and temperature. *Colloids and Surfaces A: Physicochemical and Engineering Aspects* 2009, 339:159-166.
66. Mak S-Y, Chen D-H. Fast adsorption of methylene blue on polyacrylic acid-bound iron oxide magnetic nanoparticles. *Dyes and Pigments* 2004, 61:93-98.

Graphical Abstract

Silica coated Fe_3O_4 magnetic nano particles functionalized with APTES and β–CD-OTS as an adsorbent for the removal of Lead (II) and Copper (II) ions from aqueous solutions